Annals of Botany **121**: 525–534, 2018
doi:10.1093/aob/mcx185, available online at www.academic.oup.com/aob

ANNALS OF BOTANY
Founded 1887

Two-stage patterning dynamics in conifer cotyledon whorl morphogenesis

David M. Holloway[1,2]*, Ignacio Rozada[1]† and Joshua J. H. Bray[3]

[1]Mathematics Department, British Columbia Institute of Technology, Burnaby, B.C., Canada, [2]Biology Department, University of Victoria, Victoria, B.C., Canada and [3]Biotechnology Program, British Columbia Institute of Technology, Burnaby, B.C., Canada
**For correspondence. E-mail David_Holloway@bcit.ca*
† Present address: B.C. Centre for Excellence in HIV/AIDS, St. Paul's Hospital, Vancouver, B.C., Canada.

Received: 31 July 2017 Returned for revision: 12 October 2017 Editorial decision: 23 October 2017 Accepted: 16 November 2017
Published electronically: 4 January 2018

• **Background and Aims** Conifer embryos, unlike those of monocots or dicots, have variable numbers of cotyledons, even within the same species. Cotyledons form in a single whorl on a dome-shaped embryo. The closely spaced cotyledons are not found outside this ring, indicating a radial control on where they can form. Polar transport of the hormone auxin affects outgrowth of distinct cotyledons, but not the radial aspect of the whorl or the within-whorl spacing between cotyledons. A quantitative model of plant growth regulator patterning is needed to understand the dynamics of this complex morphogenetic process.
• **Methods** A two-stage reaction–diffusion model is developed for the spatial patterning of growth regulators on the embryo surface, with a radial pattern (P1) constraining the shorter-wavelength cotyledon pattern (P2) to a whorl. These patterns drive three-dimensional (3-D) morphogenesis by catalysing local surface growth.
• **Key Results** Growth driven by P2 generates single whorls across the experimentally observed range of two to 11 cotyledons, as well as the circularly symmetric response to auxin transport interference. These computations are the first corroboration of earlier theoretical proposals for hierarchical control of whorl formation. The model generates the linear relationship between cotyledon number and embryo diameter observed experimentally. This accounts for normal integer cotyledon number selection, as well as the less common cotyledon fusings and splittings observed experimentally. Flattening of the embryo during development may affect the upward outgrowth angle of the cotyledons.
• **Conclusions** Cotyledon morphogenesis is more complex geometrically in conifers than in angiosperms, involving 2-D patterning which deforms a surface in three dimensions. This work develops a quantitative framework for understanding the growth and patterning dynamics involved in conifer cotyledon development, and applies more generally to the morphogenesis of whorls with many primordia.

Keywords: Conifer; Pinaceae; embryogenesis; whorl; cotyledon; pattern formation; morphogenesis; finite element model; plant growth regulator; reaction–diffusion; auxin; NPA

INTRODUCTION

Angiosperm monocots and dicots are tightly constrained to form one or two cotyledons, respectively. By contrast, Pinaceae conifers can have highly variable numbers of cotyledons (n_c), both between and within species (von Aderkas, 2002). Average n_c for species are reported as low as 3 (in *Tsuga*) and as high as 9 (in *Cedrus*) (Butts and Buchholz, 1940). Within species, n_c typically ranges ±1 from these averages for zygotic embryos (Butts and Buchholz, 1940). For somatic cultures (of clonal lines), embryos with n_c from 3 to 10 are common in *Larix*, *Pseudotsuga* and *Picea*, which have species averages of 5 to 6 (Harrison and von Aderkas, 2004; Holloway *et al.*, 2016).

The positioning of three or more cotyledons on an embryo is geometrically more complex than is the case for monocots or dicots, in which the most complex arrangement defines a one-dimensional (1-D) line between two cotyledons. By contrast, three or more cotyledons can be arranged two-dimensionally (on the embryo surface), and patterned either regularly or irregularly. With this additional complexity, and without the rigid constraint on cotyledon number seen in angiosperms, conifer cotyledon formation can provide unique insights into the developmental mechanisms for the spatial positioning of organs.

Among the possibilities for 2-D patterning, conifer cotyledons notably do not form all over the surface, but arise simultaneously in a single whorl (Fig. 1C). For the circular geometries involved – embryos go from a domed (Fig. 1A) to a flattened shape (Fig. 1B) during cotyledon development – formation of the whorl indicates pattern control along the radial dimension (Fig. 1E, 'r': distance on the surface from the embryo tip or centre, or 'latitude' on a hemisphere). Within this whorl, regular cotyledon-to-cotyledon spacing (Fig. 1C, 'λ') indicates pattern control in the circumferential dimension (Fig. 1E, 'φ': 'longitude' on the hemisphere). The linear variation of n_c with diameter expected for regular spacing in a ring (Fig. 1E, black spots) has been found experimentally in *Larix* (Harrison and von Aderkas, 2004), *Pseudotsuga* and *Picea* (Holloway *et al.*, 2016), indicating that n_c variability reflects embryo-to-embryo

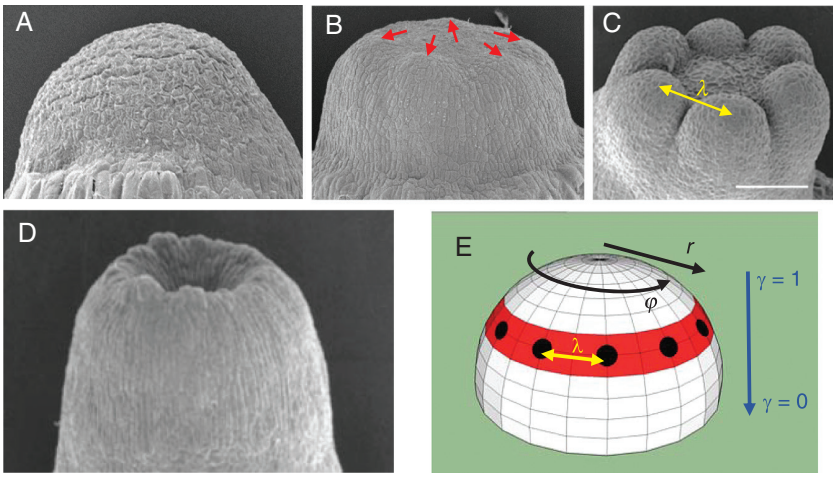

FIG. 1. Cotyledon patterning in conifer development. (A) An early dome-shaped embryo. (B) At a later stage, embryos have flattened and cotyledons are just beginning to appear (red arrows). (C) Cotyledons subsequently grow out, in a whorled (ring) pattern, with a distinct inter-cotyledon spacing, λ. Scale bar = 200 μm. (D) Cup-shaped embryos, with no distinct cotyledons, can occur spontaneously or be induced by NPA treatment (blocking polar auxin transport). This indicates two linked patterning events (E): the first (pattern P1, red) controlling the radius (*r* coordinate) of the cotyledon ring (or its 'latitude' on the dome); the second (pattern P2, black spots) controlling the spacing, λ, between cotyledons in the ring (along φ, the circumferential coordinate, or 'longitude' on the dome). P2 patterning is disrupted in cup-shaped embryos. γ denotes the flatness of the embryo (as defined in Nagata *et al.*, 2013: γ = 1, hemisphere; γ = 0, flat disc). A–C and E are adapted from Holloway *et al.* (2016), D from Harrison and von Aderkas (2004), with permission. (A–D) Larch (*Larix*) embryos are shown.

diameter variability. Without radial constraint, the short wavelength cotyledon spacing (λ) would position cotyledons over the entire embryo, which is not observed: arrangement of primordia in a single whorl involves the combination of a longer spatial scale radial control with a shorter scale circumferential control.

In conifers, the radial and circumferential aspects of cotyledon outgrowth are experimentally separable: disrupting transport of the hormone auxin with NPA (1-*N*-naphthylphthalamic acid) results in loss of circumferential patterning (Larsson *et al.*, 2008; Hakman *et al.*, 2009), producing circularly symmetric cup-shaped embryos which lack distinct, separated cotyledons (Fig. 1D).

In this paper, we develop a quantitative model for conifer cotyledon positioning, in order to create a framework for understanding the dynamics involved in normal development as well as in response to NPA treatment. The model is two-stage, with mechanisms for radial positioning (pattern 1, P1; red, Fig. 1E) and for the circumferential between-cotyledon positioning (pattern 2, P2; λ, Fig. 1E). The mechanisms are linked hierarchically: P1 control of where the short-wavelength P2 pattern occurs provides the radial constraint necessary for cotyledon whorl formation. NPA affects P2-patterned cotyledon outgrowth, not the circularly symmetric P1 component.

To couple the spatial patterning to embryo shape change, the surface is grown in proportion to the local P1/P2 concentrations; i.e., the P1/P2 mechanism models the dynamic distribution of plant growth regulators corresponding to whorl morphogenesis. As size and geometry changes of the surface in turn affect spatial patterning, the model is 'morphodynamic' (Salazar-Ciudad *et al.*, 2003), encompassing the full feedback cycle between growth regulator patterning and surface deformations. The P1 and P2 patterns are stable to this induced growth, as well as being stable over experimental ranges of embryo diameters and to the geometric flattening occurring during cotyledon formation.

Turing (1952) proposed the first mathematical model for chemical pattern formation, which he and subsequent researchers applied to spatial patterning in plant development. His reaction–diffusion (RD) theory shows how reactions between two or more chemicals (morphogens) having unequal diffusivities can self-organize stable concentration waves with a characteristic spacing or wavelength. RD patterns have been confirmed in the development of both animals (e.g. Sick *et al.*, 2006; Sheth *et al.*, 2012; Raspopovic *et al.*, 2014) and plants (e.g. Digiuni *et al.*, 2008). RD has been applied to many cases of plant development, both for 'morphostatic' (Salazar-Ciudad *et al.*, 2003) patterning on growing domains (e.g. Harrison *et al.*, 1981; Meinhardt, 1982; Jönsson *et al.*, 2005; Digiuni *et al.*, 2008; Fujita *et al.*, 2011) and for 'morphodynamic' patterning of growth regulators driving morphogenesis (Harrison and Kolář, 1988; Holloway and Harrison, 1999, 2008). In RD, chemical transport is via simple diffusion down a concentration gradient.

More recently, it has been discovered that the growth regulator auxin has unique intercellular transport properties (reviewed by Friml, 2003). In addition to simple diffusion, auxin has its own cellular efflux transporters, PIN proteins. Localization of PINs to subregions of the cell membrane produces a polar auxin transport (PAT). PAT, in conjunction with simple diffusion, can self-organize auxin concentration patterns (shown analytically, for example, by Jönsson *et al.*, 2006; Draelants *et al.*, 2013; Farcot and Yuan, 2013). PAT can include a with-the-flux localization of PIN1 (a down-the-gradient facilitated diffusion), which has been applied to canalization and venation (e.g. Mitchison, 1981; Rolland-Lagan and Prusinkiewicz, 2005; Feugier *et al.*, 2005), or an up-the-gradient localization of PIN1, which has been applied to the sequential placement of organs in phyllotaxis (e.g. Jönsson, *et al.*, 2006; de Reuille *et al.*, 2006; Smith *et al.*, 2006). Models of complex auxin patterning, such as for phyllotaxis plus venation, can include terms for intracellular reactions, simple diffusion, up-the-gradient PAT and down-the-gradient PAT (e.g. Bayer *et al.*, 2009). Such

mechanisms can have very complex dynamics, because even subsets of the terms – such as reaction and diffusion (Turing, 1952), or diffusion and up-the-gradient PAT (e.g. Jönsson, *et al.*, 2006) – are capable of self-organization.

Previous models of whorled phyllotaxis have focused on the successive formation of whorls, and have defined organ initiation at a fixed radius R_0 from the centre of an apical or floral meristem (Douady and Couder, 1996; Kitazawa and Fujimoto, 2015). In these models, the occurrence of whorls (as compared to spirals) depends on R_0 and on the timing and size of sequential primordia initiation. Initiation sites are affected by the positions of older primordia. In conifer embryos, however, a single whorl of cotyledons forms simultaneously, and the single whorl is robust to large changes in radius: experimental measurements show whorl radii increase by about 150 µm over the range of observed n_c (Holloway *et al.*, 2016; whorl radius is approx. 125 µm less than embryo radius). This indicates an adaptive self-organizing P1 mechanism (in the *r* coordinate) to position the single cotyledon whorl 150 µm closer to the centre in small embryos with low n_c than in large embryos with high n_c, and argues against a fixed radius R_0 (for instance set by diffusion of a morphogen from the embryo centre), which would not adapt to embryo size variation as observed.

The induction of cup-shaped embryos by NPA treatment indicates a PAT dependence for the circumferential P2 cotyledon pattern (along the φ coordinate), but not for the circularly symmetric P1 ring pattern. Turing dynamics in intracellular reactions and simple diffusion can self-organize pattern in the absence of PAT dynamics. RD is therefore used as a framework for quantitatively characterizing the PAT-independent P1 pattern. This is similar to the recent application of RD dynamics to the radial control of shoot apical meristem size (Fujita *et al.*, 2011). Quantifying radial patterning in this way allows us to characterize the dynamics involved in forming a single whorl robust to the wide range of embryo sizes found in conifers.

For the circumferential P2 pattern, the NPA effect appears to be primarily on the outgrowth of cotyledons: while most embryos do not grow cotyledons at moderate NPA concentrations, those that do tend to show normal circumferential spacing (Holloway *et al.*, 2016). This indicates that the *outgrowth* of distinct cotyledons from the ring is PAT-dependent (perhaps via supply of a critical factor), but that the *spacing* λ between cotyledons is PAT-independent. In wave terminology, PAT appears to affect P2 amplitude, not its wavelength. We therefore use a PAT-independent RD mechanism to model self-organization of the P2 cotyledon–cotyledon wavelength λ. The NPA effect on P2 amplitude is modelled as a PAT-dependent factor that affects whether the RD mechanism can actively form a pattern.

While RD can be used to study *de novo* pattern formation from an unpatterned state, the more common occurrence in development is for patterns to form on prior patterns, as with the P1/P2 stages studied here. Harrison *et al.* (1981) first proposed such hierarchical patterning for whorl formation in the alga *Acetabularia*, with subsequent experiments indicating that RD was involved in circumferential spacing in the whorl (Harrison *et al.*, 1988, 1997). Turing identified RD parameter conditions for spatial patterns to grow (amplify) from initially uniform concentration states (PAT models can be analysed similarly). We refer to this self-organizing generation of new pattern as **active** patterning. RD can also generate active pattern from a pre-patterned state (termed 'Turing models of the 2nd kind', Hunding, 1987); in these cases the pre-pattern limits where the RD pattern forms (by controlling where the Turing conditions are met for active patterning, although linear Turing analysis is an approximation with pre-patterns). For the conifer model, P1 controls where P2 can actively generate the circumferential cotyledon pattern. However, when conditions do not support P2 active patterning (e.g. if a critical factor is affected by NPA reduction of PAT), P2 relaxes to a **passive** pattern: this is not a uniform concentration, but rather reflects the radial P1 ring pattern.

The P1/P2 model for patterning and morphogenesis allows us to quantify the dynamic constraints involved in forming conifer cotyledon whorls. For patterning, these include constraints on reaction and transport kinetics, the response to NPA interference with PAT, and how the P1 and P2 stages are coupled. For morphogenesis, these include constraints on P1/P2 catalysed surface growth, the effect of that growth on patterning and the effect of 3-D embryo geometry on morphogenesis. The model provides a framework for interpreting current data and guiding new experiments to understand conifer cotyledon development and the establishment of whorled structures in general.

MODEL AND METHODS

As discussed above, the P1 and P2 spatial patterns are each generated by an RD mechanism. The annular P1 pattern specifies the radial position at which cotyledons form. P1 affects a rate constant in the P2 mechanism, constraining the P2 circumferential patterning to this ring. P2 is morphogenetic, altering 3-D shape by locally catalysing surface growth.

The Brusselator RD mechanism (Prigogine and Lefever, 1968) is used for the P1 pattern:

$$\frac{\partial X_1}{\partial t} = a_1 A_1 - b_1 B_1 X_1 + c_1 X_1^2 Y_1 - d_1 X_1 + D_{X_1} \nabla^2 X_1 \quad (1a)$$

$$\frac{\partial Y_1}{\partial t} = b_1 B_1 X_1 - c_1 X_1^2 Y_1 + D_{Y_1} \nabla^2 Y_1 \quad (1b)$$

where X_1 and Y_1 are the concentrations of the spatially patterned Turing morphogens (subscript 1 for P1). *A* and *B* are precursor concentrations; *a*, *b*, *c* and *d* are reaction rate constants; and the final terms are for diffusion of X_1 and Y_1 with diffusivities D_{X1} and D_{Y1}, respectively. X_1 self-amplifies (cX^2Y term), but this increase is limited by using up Y_1. This depletion-type kinetics tends to form regular patterns in X_1 and Y_1 very close to predictions from linear analysis (e.g. Lacalli, 1981; Harrison, 1993; Holloway and Harrison, 1995) and has been used extensively for regular branching processes in morphogenesis (Harrison and Kolář, 1988; Holloway and Harrison, 1999, 2008; Nagata *et al.*, 2003, 2013; Jönsson *et al.*, 2005; Rozada *et al.*, 2013). Due to this regularity, the Brusselator was used to model formation of the P1 annulus (Fig. 2D, G).

The depletion kinetics of the Brusselator, however, make it unsuitable for a P2 pattern, which is controlled by P1. Without loss of generality, *a*, *b*, *c* and *d* can be set to unity, and the *A* and *B* concentrations become the only reaction parameters in the model (Nicolis and Prigogine, 1977). A feedforward from P1 to a P2 Brusselator could be made by identifying one of

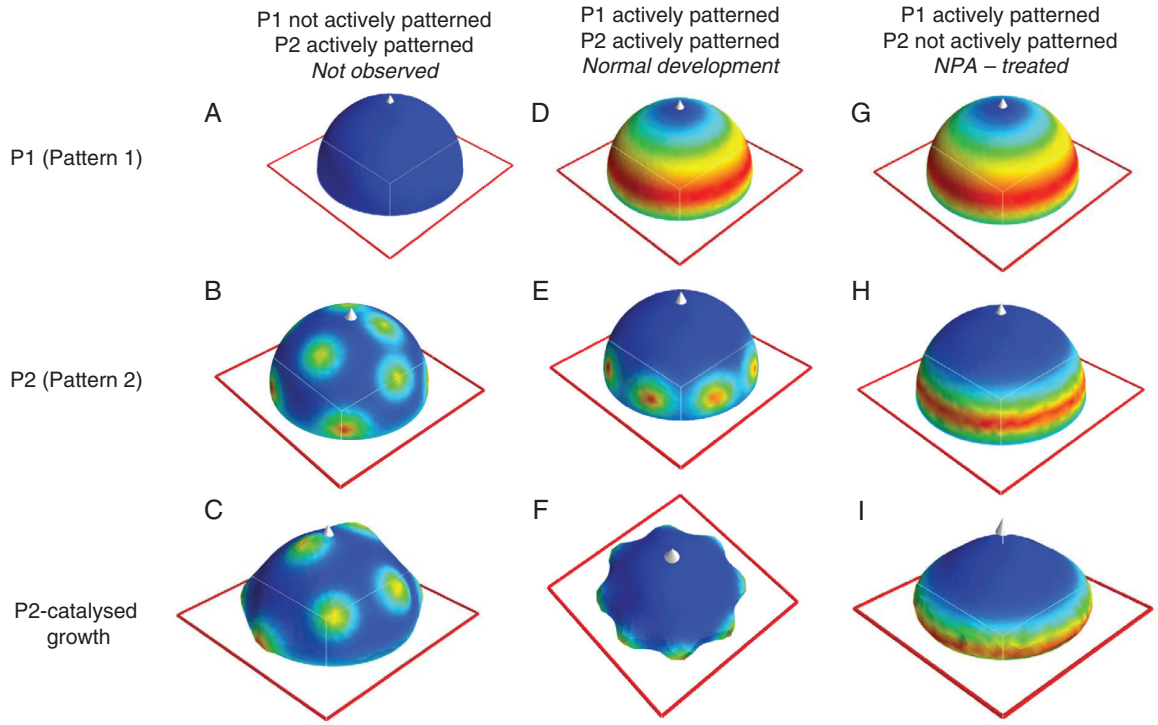

FIG. 2. Two-stage model for conifer cotyledon morphogenesis. Top row, spatial pattern 1 (P1), colour-mapped for morphogen X_1; middle row, spatial pattern 2 (P2), colour-mapped for morphogen X_2; bottom row, 3-D shape generated by X_2-catalysed growth (colour-mapped for X_2). The top two rows are hemispherical surfaces, while the shapes on the bottom row grow from initial hemispheres. Red outlines are in the x–y plane; white arrow, z-axis. P1 and P2 patterns are generated by reaction–diffusion (RD) mechanisms (eqns 1 and 2, respectively); X_1 and X_2 concentrations are shown colour-mapped from blue (lowest concentration) to red (highest concentration). The X_1 concentration (top row) affects a production rate constant in P2 (eqn 3), constraining where P2 forms (middle row). (A–C) When P1 is not actively patterned, X_1 (A) and Y_1 revert to uniform steady-state concentrations. This allows the short-wavelength P2 pattern to form all over the domain (B), catalysing a 'spots-all-over' bumpy morphogenesis (C), which is not seen in conifer embryogenesis. (D–F) When P1 is actively patterned, X_1 forms a ring defining the radial position of the cotyledon whorl (D). This (by eqn 3) constrains P2 to form only within the ring (E). Outgrowth of regularly spaced primordia corresponds to normal cotyledon morphogenesis (F). (G–I) If P2 is not actively patterning, it has a steady-state pattern (H) which follows that of P1 (G), and outgrowth is circularly symmetric (I), like NPA-treated cup-shaped morphogenesis.

the P1 morphogens (X_1 or Y_1) with the A_2 or B_2 precursors for P2. This P1-patterned feedforward must be into A_2 to produce a passive P2 ring pattern when simulating NPA treatment, as the passive steady state of X_2 is proportional to A_2 and does not depend on B_2. However, active patterning happens at **low** A in the Brusselator (Herschkowitz-Kaufman, 1975), which contradicts forming P2 concentration peaks in the high A_2 annulus specified by P1. That is, such a mechanism cannot form active normal cotyledon pattern in the same radial position as the passive NPA-treated ring, as is observed experimentally.

We therefore used an activator–inhibitor kinetic mechanism in which both active and passive P2 pattern are in-phase with the P1 annulus (Fig. 2E, H). This Gierer–Meinhardt (GM) mechanism (Gierer and Meinhardt, 1972) is given by:

$$\frac{\partial X_2}{\partial t} = a_2 A_2 + \frac{c_2 A_2 {X_2}^2}{Y_2} - d_2 X_2 + D_{X_2} \nabla^2 X_2 \qquad (2a)$$

$$\frac{\partial Y_2}{\partial t} = b_2 B_2 {X_2}^2 - e_2 Y_2 + D_{Y_2} \nabla^2 Y_2 \qquad (2b)$$

for the morphogens X_2 and Y_2, with subscript 2 for P2.

P1 to P2 feedforward is implemented by setting

$$c_2 = nX_1 \qquad (3)$$

as gradients in c_2 strongly affect GM pattern localization (Holloway and Harrison, 1995). Equations (1)–(3) establish the necessary chemical prepatterns for morphogenesis of a single simultaneously initiated whorl of primordia (Fig. 2D–F).

Equations (1)–(3) were solved by an implementation of the finite element method (FEM) in Python (version 2.7.3), using the Fenics 1.5 (https://fenicsproject.org/; Logg and Wells, 2010; Logg *et al.*, 2012; Alnaes *et al.*, 2015), numpy (http://www.numpy.org/) and scipy (https://www.scipy.org/) libraries. Mayavi2 graphics were used for visualization (http://mayavi.sourceforge.net/). The initial triangulated mesh specifying the surface was generated by gmsh 2.5.1 (http://gmsh.info/). Initial shapes were hemispherical caps, specified by flatness parameter γ between 1 (hemisphere) and 0 (flat disc) (see Fig. 1E). Initial surfaces were defined on between 793 and 801 vertices (exact value depended on the radius specified). All surfaces had 65 boundary (equatorial) vertices, but surfaces with $\gamma < 1$ had fewer total vertices than $\gamma = 1$ at any given radius, in proportion to the decrease in pole height. Boundary conditions were fixed-value (Dirichlet), with X and Y concentrations (eqns 1 and 2) specified as their passive steady-state values (X_0, Y_0) on the boundary (equatorial positions). (No-flux boundary conditions would create maxima at the pole or equator, which would not correspond to the observed whorls.)

To couple this prepattern to morphogenesis, local growth of the surface was implemented as in Harrison *et al.* (2001) and Holloway and Harrison (2008): in each iteration, finite elements intersecting at a mesh vertex were increased in area proportional to the local X_2 concentration; mesh vertices were then moved along the local normal vector (averaged from the normals of the neighbouring finite elements) to accommodate this area change (e.g. Fig. 2C, F, I). Vertex positions were updated simultaneously for the whole surface. Boundary (equatorial) vertices had fixed positions.

The spatial solutions of eqn (1) (or any pattern-forming mechanism) on a hemispherical geometry are composed of the surface spherical harmonics, $Y(m,l)$, which are polynomials with m repeated structures in the φ dimension (longitude) and l latitudes at which the solution passes through the passive steady-state value. Occurrence of the P1 ring depends on the fit between the domain (embryo) size and the spacing of the chemical patterning mechanism (wavelength). The parameters in Table 1 (reaction rate constants from Holloway and Harrison, 2008) generate a P1 Y(0,3) ring pattern (e.g. Fig. 2D, G) which is stable over more than a doubling of domain radius, or, equivalently, to a more than halving of pattern spacing. This represents robustness to at least a factor of two change in reaction or diffusion constants (since these have a less than linear effect on RD spacing; Harrison, 2011, chapter 5).

GM (eqn 2) reaction rate parameters are as in Holloway and Harrison (1995), except for initial $c_2 = 0.005$ (for $t > 0$, c_2 follows eqn 3), with diffusivities selected to give a wavelength $\lambda = 0.52$ (calculated from linear analysis), corresponding to 12 P2 primordia at radius 1 (and $\gamma = 1$). The feedforward constant n (eqn 3) scales X_1 to keep P2 in the active patterning region of the linear parameter space. NPA treatment is simulated by reduction of d_2, which shuts off active P2 patterning without strongly affecting wavelength (Holloway and Harrison, 1995). Linear analysis predicts this qualitative active-to-passive change for decreasing d_2; numerical simulations were used to find this boundary value for the non-linear system of eqns (1) and (2). Local growth is proportional to X_2 (parameter c_g), and is calculated once for every 50 iterations (of size Δt) of the RD solver. Simulations were run for 30 000 iterations.

RESULTS

Whorl formation: P1 constraint of P2

Lack of constraint. An essential feature of single whorl formation is that a relatively short wavelength spacing (the inter-cotyledon λ shown in Fig. 1) is constrained to a ring. In the absence of a radial (or latitudinal) constraint, a mechanism with such a short wavelength would generate pattern all over the domain. This is illustrated in Fig. 2A–C, in which active patterning is turned off in the P1 Brusselator (by setting diffusivities D_{X1} and D_{Y1} to zero), resulting in unpatterned, uniform X_1 and Y_1 concentrations (Fig. 2A). Active patterning in P2 is then spatially unconstrained, and concentration peaks form all over the surface (Fig. 2B). If this P2 pattern catalyses surface expansion, outgrowths occur over the whole domain (Fig. 2C): this is not observed in conifer cotyledon morphogenesis (or single whorl morphogenesis in general).

Normal patterning and morphogenesis. With P1 actively patterning and generating a relatively long-wavelength annular pattern (Fig. 2D), feedforward (eqn 3) constrains the short-wavelength P2 to form in a whorl and not over the centre of the domain (Fig. 2E). Growth catalysed by P2 generates the regularly spaced whorl of primordia associated with normal cotyledon morphogenesis (Fig. 2F). Equations (1)–(3) provide a framework for the dynamics needed for the morphogenesis of a single simultaneous whorl of primordia.

Table 1. *Model parameters*

Equation (1)	Equation (2)	Other
$\boldsymbol{a_1 = 0.01}$	$a_2 = 0.0006$	$n = 0.00125$
$\boldsymbol{b_1 = 1.5}$	$b_2 = 0.025$	$c_g = 0.001$
$\boldsymbol{c_1 = 1.8}$	$c_2 = 0.005$ (initial)	$\Delta t = 0.01$
$\boldsymbol{d_1 = 0.07}$	d_2 (normal) = 0.21; d_2 (NPA) = 0.14	Number of vertices ($\gamma = 1$) ~ 800
	$e_2 = 0.27$	
$\boldsymbol{A_1 = 10.0}$	$A_2 = 0.4$	
$\boldsymbol{B_1 = 1.0}$	$B_2 = 0.4$	
$\boldsymbol{D_{X1} = 0.01}$	$D_{X2} = 0.0004$	
$\boldsymbol{D_{Y1} = 0.1}$	$D_{Y2} = 0.008$	

NPA effect on P2 patterning

Cup-shaped morphogenesis (spontaneous or due to NPA treatment) is associated with loss of P2 patterning (lack of distinct cotyledon outgrowth). With normal active P1 patterning (Fig. 2G), loss of active P2 patterning reverts to a passive steady state reflecting the P1 annular pattern (Fig. 2H). The PAT-dependent shut-off of P2 self-organization is modelled via reduction of the decay parameter d_2, from 0.21 (normal) to 0.14 (NPA-treated). Growth catalysed by the resulting annular passive P2 pattern generates the circularly symmetric morphogenesis of cup-shaped embryos (Fig. 2I). Partial reduction of d_2, to 0.18, produces active P2 pattern, but at lower amplitude than normal. This corresponds to the decreased amplitude outgrowth but relatively unaffected P2 spacing observed experimentally under moderate NPA treatments (Holloway *et al.*, 2016).

Effect of geometry on morphogenesis

Cotyledons *in vivo* tend to point upwards (Fig. 1C), and this upwards tendency is retained even in cup-shaped embryos lacking cotyledons (Fig. 1D). The radial location of the P1 ring on the dome could potentially affect this outgrowth angle, with higher latitude rings giving smaller angles between the outgrowth and the z-axis. The single-ring solution of the P1 eqn (1) on a hemispherical cap is the annular Y(0,3) surface spherical harmonic (Fig. 2D, G), which has a characteristic inset from the equator. Higher latitude rings could arise for higher-order harmonics (e.g. Y(0,7)), but this would also produce multiple rings, which are not seen in normal conifer development.

Geometry could also contribute to upward growth. Flattening of a hemispherical geometry, as seen during conifer embryogenesis (Fig. 1A to Fig. 1B), decreases the angles between the z-axis and normal vectors on the surface. Therefore, P1 patterning on a flattened dome should direct more upwards growth than on a hemisphere. To test this geometric effect, we ran

series of computations at different values of γ, the parameter specifying dome flatness (varying between 1 for a hemisphere and 0 for a flat disc; see Fig. 1E and Nagata *et al.*, 2013). Figure 3 compares morphogenesis from hemispherical initial shapes (Fig. 3A, B) to increasingly flat initial shapes (Fig. 3C, D to Fig. 3E, F). Decreasing γ decreases the outgrowth angle from the *z*-axis, producing closer fits to observations, both for cotyledon outgrowth and for NPA-induced cups. This indicates that establishment of the P1 pattern on geometries intermediate between a hemisphere (γ = 1) and a flattened disc (γ = 0), i.e. patterning after the dome stage (Fig. 1A), could contribute to the observed upwards growth.

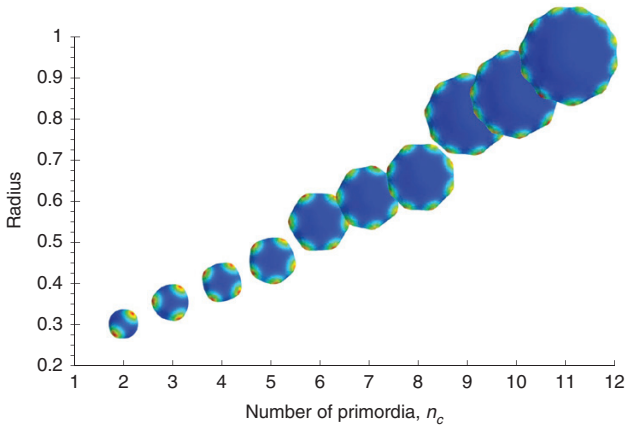

FIG. 4. Linear relationship between number of primordia (n_c) and radius, as predicted from eqn (4) and corresponding to the trend seen experimentally (Harrison and von Aderkas, 2004; Holloway *et al.*, 2016). Top-view shapes, colour-mapped for X_2 concentration, shown to scale. The P1 ring stabilizes formation of a single whorl of primordia over the observed range of two to 11 cotyledons (Holloway *et al*, 2016). γ = 0.8 with X_2-catalysed growth is shown; see Table 2 for the linear relationship at other geometries.

Linear relation between primordia number and diameter

A characteristic wavelength, λ, for P2 spacing within the P1 ring implies a linear relationship between domain diameter, *d*, and the number of primordia, n_c:

$$d = (\lambda/\pi)n_c + b \qquad (4)$$

where *b*/2 is the inset of the ring from the equator. This relationship is seen experimentally (Harrison and von Aderkas, 2004; Holloway *et al.*, 2016). For the P1/P2 RD simulations, Fig. 4 shows this linear increase in radius with primordia number. The linear trend is observed at different γ values, and with or without P2-catalysed growth (Table 2; $P < 0.05$ for all regressions).

The single ring of primordia is stable across the two to 11 cotyledons observed experimentally. This stability of whorl formation depends on P1 pattern stability with respect to radius increase. Spatial solutions of dynamic mechanisms such as eqn (1) depend on domain size, with a progression from lower to higher complexity patterns as size increases. At small radius, the domain size is too small for the annular Y(0,3) spherical harmonic: P1 forms a lower-order, pole-high Y(0,1) pattern in these cases. P2 can form n_c = 2 to 4 on these small-radius P1 patterns (Table 2, yellow). This is consistent with previous results, in which we observed whorl patterns up to n_c = 6 for a single Brusselator pattern-former on a Y(0,1) fixed pre-pattern (Holloway and Harrison, 2008). For larger radii, however, the Y(0,3) annular pattern generated by the dynamic P1 mechanism (as in Fig. 2 D, G) is critical for stabilizing P2 whorl formation (as compared to 'spots all over', e.g. Fig. 2B). The P1 annulus stabilizes whorls to the upper end of the experimentally observed range: up to n_c = 11 is shown in Table 2 (green and blue); n_c = 12 and 13, of which single cases were observed in Holloway *et al.* (2016), can also be generated. At higher radii

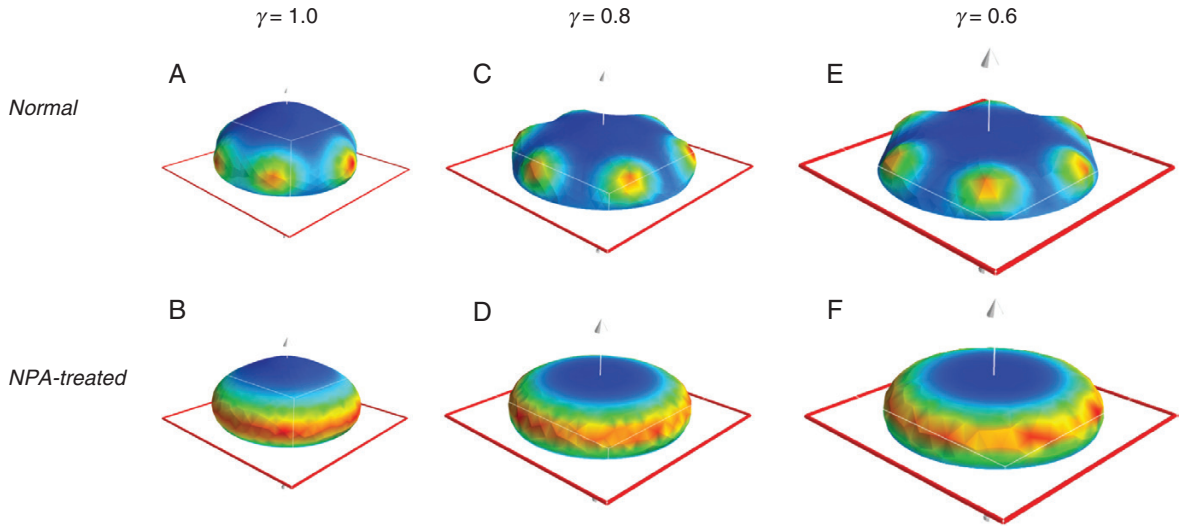

FIG. 3. The effect of geometry on patterning and morphogenesis. Top row, normal morphogenesis (both P1 and P2 actively patterning); bottom row, NPA-treated cup morphogenesis (P1 actively patterning, P2 not actively patterning). Colour-map, red outline and white arrow as in Fig. 2. (A, B) Growth starting from hemispherical initial shapes, γ = 1.0 (see Fig. 1E legend). (C–E) Progressively flattened domains: (C, D) γ = 0.8; (E, F) γ = 0.6, shown to scale. The radius increase as γ decreases keeps the number of primordia (6, here) constant. As the domain flattens, the angle between the *z*-axis (pole) and the P1 ring decreases, directing the primordia upwards, more closely matching the observed morphogenesis (Fig. 1C). This corresponds to cotyledons being positioned during tip flattening, after the dome stage (Fig. 1A) of embryogenesis.

TABLE 2. *Initial radii at particular number of primordia* n_c, *for different tip flatness* γ

	n_c									
	2	3	4	5	6	7	8	9	10	11
$\gamma = 1$										
Growth	0.2	0.25	0.325	0.375	0.4	0.5	0.6	0.65	0.7	0.8
No growth	0.25	0.275	0.3	0.4	0.45	0.5	0.6	0.7	0.8	0.85
$\gamma = 0.8$										
Growth	0.3	0.35	0.4	0.45	0.55	0.6	0.65	0.8	0.85	0.95
No growth	0.3	0.35	0.4	0.45	0.55	0.6	0.7	0.79	0.8	0.95
$\gamma = 0.6$										
Growth	0.3	0.4	0.45	0.5	0.6	0.665	0.7	0.8	0.9	1.0
No growth	0.35	0.4	0.5	0.55	0.59	0.65	0.75	0.9	0.95	1.0

Yellow – Y(0,1) P1 pattern; green – faint Y(0,3) P1 pattern; blue – sharp Y(0,3) P1 pattern. No growth: fixed hemispherical cap geometry for all time ≥ 0. Growth: same initial geometry, but with X_2-catalysed surface growth for time > 0.

than these, P1 begins to transition to a multiple ring Y(0,7) pattern, which would correspond to radially nested P2 whorls, which are not seen in normal development. Simulation of NPA treatment, decreasing d_2 to shut off active P2 patterning, gave circularly symmetric morphologies for all radii in Fig. 4.

Variations in patterning

Transitions between distinct patterns can be gradual for P1 and P2. In Table 2, for instance, the P1 transition between the Y(0,1) pole-high and Y(0,3) annular patterns occurs over a range of radii (green cells), with the Y(0,3) polar minima becoming more distinct as radius increases. For P2, radii between those shown in Table 2 can give mixed patterns, resulting in either splittings (e.g. an initial $n_c = 4$ going to $n_c = 5$, Fig. 5A) or fusions (long circumferentially extended maxima which fail to resolve into distinct primordia, Fig. 5B). Splittings are seen experimentally, for example with an embryo showing four cotyledons on an initial measurement showing five cotyledons a week later. Fusions are also observed, where, for example, space for two cotyledons is occupied by a single broad structure (Fig. 5C). The simulations indicate that such indeterminate n_c could be a natural consequence of the radial dependence of the P2 pattern, i.e. that these embryos are at a transitional size between radii with distinct integer n_c.

NPA treatment tends to abolish outgrowth of distinct cotyledons, but in rare cases vestigial 'bumps' can be observed along the rims of the cup-shaped embryos (Holloway *et al.*, 2016). Since NPA treatment appears to reduce P2 amplitude without altering the P2 spacing λ, these bumps may be due to a remaining very low-amplitude P2 pattern during their development.

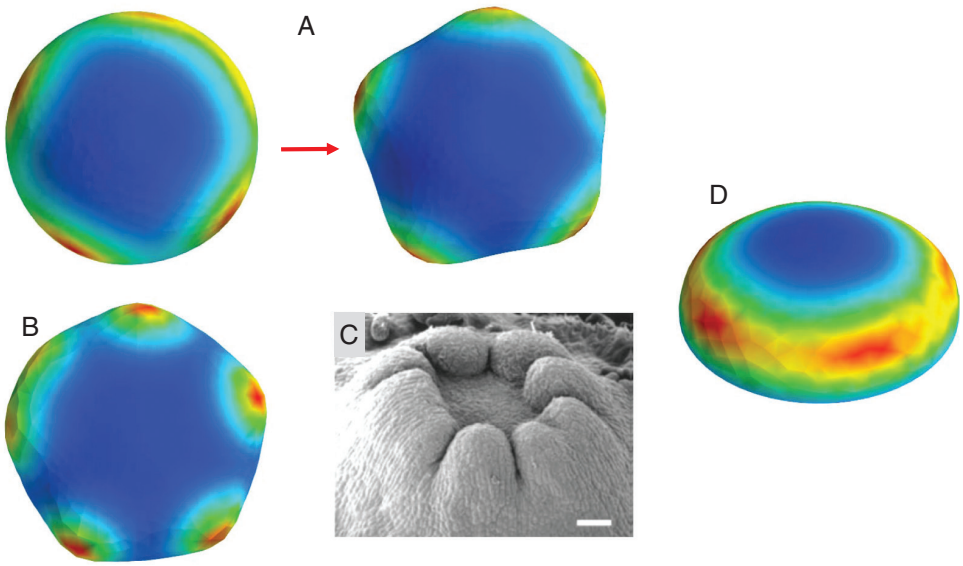

FIG. 5. Variation in patterns. The model can generate some of the anomalous morphologies seen experimentally. (A) Concentration peak splitting, in this case from an earlier pattern of four peaks (left) to a later pattern of five peaks (right), corresponds to readjustments seen experimentally, where additional cotyledons are sometimes seen a week after the earliest count. (B) Peak fusions, where a ring with space for, in this case, between five and six peaks, has several peaks 'smeared' together, corresponding to fused or extra-width cotyledons sometimes observed experimentally (C; from Harrison and von Aderkas, 2004, with permission; scale bar = 250 μm). Such cases of indistinct peak number tend to occur at transitional radii between distinct integer peak numbers (i.e. between the shapes shown in Fig. 4). (D) Transient pattern in early stages of an 'NPA-treatment' simulation (at later stages, this passive P2 pattern is distributed in a smooth ring). Such transient pattern could correspond to the 'bumpy cup' morphology sometimes observed in NPA-treated embryos, where the cup rim is not smooth (Holloway *et al.*, 2016).

Figure 5D shows that in cases where P2 is not actively patterning, and has a steady state which will follow the P1 annular pattern, transient circumferential pattern can still be observed at early stages, which could contribute to vestigial bumps prior to the pattern fully relaxing to the annular steady state.

DISCUSSION

Cotyledon morphogenesis in conifers is complex, with positioning and outgrowth controlled in radial and circumferential directions on a flattening dome geometry. Fundamental questions in this process include: how are cotyledons constrained radially to form in a whorl; how are cotyledons evenly spaced circumferentially within that whorl; what is the role of auxin in cotyledon formation; and how do spatial patterning dynamics affect the morphology of the cotyledon crown in early embryos? We developed a dynamic model of pattern formation and growth in three dimensions to investigate these questions.

Induction of cup-shaped morphogenesis by NPA treatment suggests that an underlying PAT-independent patterning mechanism, P1, sets the radial position of the cotyledon whorl. This ring pattern is robust – even in NPA-treated embryos showing partial cotyledon growth or embryos with missing cotyledons (gaps), outgrowth occurs at a clear radius from the tip (Larsson *et al.*, 2008; Holloway *et al.*, 2016). The consistent formation of whorls in conifer cotyledon development depends on the stability of this single-ring pattern solution to changes in domain size, embryo geometry and mechanism parameters (e.g. reaction rates, transport rates, potentially mechanical properties). The size stability of the whorl pattern is notable in the broader developmental context, given that within-species conifer embryo sizes are far more variable (s.d./mean ≈ 30 % for diameters; Holloway *et al.*, 2016) than those in *Drosophila* (s.d./mean ≈ 8 % for lengths; Holloway *et al.*, 2006), a model organism intensively studied for such pattern scaling to variable size (e.g. Houchmandzadeh *et al.*, 2002; He *et al.*, 2015). On flattening dome geometries, the single-ring whorl pattern corresponds to the Y(0,3) spherical harmonic. We have shown that an RD P1 mechanism (the Brusselator) can stabilize single whorls across the range of two to 11 cotyledons observed experimentally. In particular, Y(0,3) P1 solutions are critical in maintaining single whorls at larger diameters. Our simulations indicate that P1 ring stabilization is important for diameters associated with $n_c > 4$; this is highly applicable to many common conifers, in which species averages are $n_c = 5$ and above (Butts and Buchholz, 1940).

To constrain cotyledon formation to the ring, P1 needs a feedforward control on the short-wavelength P2 pattern. The formation of P1 and P2 patterns in-phase in the whorl is consistent with GM activator–inhibitor kinetics for P2, and not with Brusselator depletion kinetics. P1 is coupled to P2 via the X_1 morphogen affecting the X_2 self-reinforcement rate parameter c_2. Active pattern formation by the GM P2 mechanism produces even spacing between primordia within the P1 ring. This is the first computed confirmation that a hierarchical double-RD mechanism can generate single whorl morphogenesis on a dome, as first suggested by Harrison *et al.* (1981).

The loss of distinct cotyledon outgrowth with NPA treatment indicates a PAT effect on P2 pattern amplitude. This is modelled as an effect on active vs. passive patterning, with NPA treatment (decrease of PAT) decreasing parameter d_2. At low d_2, active circumferential patterning dies out and the resulting passive steady-state of P2 reflects the underlying P1 ring pattern (Fig. 2H). Turing analysis shows how d_2 decrease causes this loss of self-organization; the decreased decay could also be associated with a pooling of unpatterned P2 morphogen in the P1 ring.

NPA-induced reversion of a distinct cotyledon pattern to a ring pattern supports the two-stage P1/P2 model over a one-stage RD model. For a single Brusselator, Nagata *et al.* (2013) found the stability conditions for different pattern harmonics on spherical caps. Transitions from cotyledon-like patterns, Y(n_c, 1), to the annular Y(0,3) would require different specific variations in parameters for each n_c. In comparison, loss of active patterning in P2 can be effected over a range of values for any of the parameters in eqn (2), more consistent with a systemic NPA treatment reliably converting all potential n_c (or all diameters, given eqn 4) to Y(0,3).

P1 control constrains a potentially 2-D P2 pattern (all over the surface) into a quasi-1-D pattern in a ring. This produces the linear dependence between inter-cotyledon spacing λ and embryo diameter (eqn 4) observed experimentally (Harrison and von Aderkas, 2004; Holloway *et al.*, 2016). In such a ring arrangement, each increment of the whorl circumference by the inter-cotyledon spacing allows another cotyledon to fit in. Table 2 shows radii for each integer n_c in the experimentally observed range. Since radius can vary continuously, radii intermediate to those shown in Table 2 can produce mixed n_c: the cotyledon fusions or splittings observed experimentally could be due to the diameter–n_c dependence contained in eqn (4).

Morphogenetically, P2-driven growth generates the evenly spaced primordia of normal cotyledon morphogenesis, as well as the circularly symmetric outgrowth of NPA-induced cup-shaped morphogenesis. The pattern formation is stable to this induced growth. Computations on different embryo geometries (dome flatness γ) suggest that P1/P2 cotyledon positioning occurs during flattening, after the early dome stage: decreasing γ from 1 (hemispherical) decreases the angle between outgrowth and the z-axis, generating increasingly upward-pointing primordia which more closely match experimental observations.

Visualization of growth regulator patterning in conifer embryos is rudimentary compared to *Arabidopsis*; the model provides a quantitative framework for interpreting the data currently available and guiding new experiments. For instance, new experiments in auxin labelling could clarify whether auxin localizes to the P1 ring, indicating a localized PAT delivery of the P2 'amplitude factor' and perhaps some dependence of PAT on P1; or whether auxin is more ubiquitous at these stages, and loss of PAT would produce a more generic loss of the P2 'amplitude factor' across the embryo. While the molecular identity of the X_2 growth catalyst is unknown at this point, the model indicates that it is patterned by activator–inhibitor kinetics, as found earlier in plants for trichome patterning (Digiuni *et al.*, 2008) and in shoot apical meristems (Fujita *et al.*, 2011).

The dynamic mechanism developed here for conifer cotyledons may apply more generally to single whorl formation in development, or to successive simultaneously forming whorls (independent of earlier primordia position) such as vegetative growth in *Acetabularia* (Dumais and Harrison, 2000) or *Equisetum*. These phenomena are in contrast to phyllotactic

whorls formed by successively initiated primordia (e.g. Douady and Couder, 1996; Kitazawa and Fujimoto, 2015), and also to the PAT self-organization model of floral whorls, in which earlier organs (sepals) affect the positioning of later organs (van Mourik *et al.*, 2012). The stability of the P1/P2 system over a large size range is especially applicable to simultaneous whorls with large numbers of primordia. In these cases, the short spacing between primordia relative to domain size requires a radial constraint to form in a whorl, and not have patterning all over the available space. While current data supports RD patterning for both P1 and P2 in conifer cotyledon whorls, the current model establishes more general constraints for whorl formation which could be realized with other pattern-forming mechanisms, such as PAT. In particular, the current model establishes constraints on the linkage between the radial and circumferential patterning systems, the coupling to growth, and the stability of the patterns to embryo size variability and geometric changes during morphogenesis: these apply to any mechanism for regular spacing, RD or otherwise.

In this broader context, the current characterization of the two-stage process in conifer cotyledon development shows parallels with previous findings of multi-component mechanisms with separable effects (and dependences on PAT) in different dimensions. These include results in tomato and *Arabidopsis*, in which exogenous application of auxin could alter circumferential patterning on the shoot, but not within a critical radial distance of the meristem (Reinhardt *et al.*, 2000); the PIN1 dependence of floral initiation compared to the partial PIN1 independence of leaf initiation (Guenot *et al.*, 2012); the separable surface and inward PAT flows found in the shoot apex (Furutani *et al.*, 2014); and the PAT-dependent lateral and PAT-independent medial components of gynoecial development (Larsson *et al.*, 2014).

Conifer polycotyledony offers a unique system for studying developmental mechanisms for the positioning of organs. Development of a 3-D finite element model of conifer cotyledon whorl formation has allowed us to study the dynamics involved in this complex morphogenetic process. This clarifies the role of the radial patterning (P1) and its stability over the size ranges found experimentally; the constraint of cotyledons to this ring; the spacing of cotyledons within the ring (P2 pattern); and the loss of P2 patterning with NPA treatment. This quantitative model for the dynamics of growth regulator patterning and consequent morphogenesis provides a synthesis of current data and can serve as a framework to guide future experiments into the molecules and mechanisms involved in conifer cotyledon development, with implications for whorl formation in general.

ACKNOWLEDGEMENTS

We thank Carol Wenzel, Patrick von Aderkas and two anonymous reviewers for comments on the manuscript; and BCIT and NSERC Canada for financial support.

LITERATURE CITED

Alnaes MS, **Blechta J**, **Hake J**, ***et al.*** **2015**. The FEniCS project version 1.5. *Archive of Numerical Software* **3**: 9–23.

Bayer EM, **Smith RS**, **Mandel T**, ***et al.*** **2009**. Integration of transport-based models for phyllotaxis and midvein formation. *Genes and Development* **23**: 373–384.

Butts D, **Buchholz JT. 1940**. Cotyledon numbers in conifers. *Transactions of the Illinois Academy of Sciences* **33**: 58–62.

de Reuille PB, **Bohn-Courseau I**, **Ljung K**, ***et al.*** **2006**. Computer simulations reveal properties of the cell–cell signalling network at the shoot apex in Arabidopsis. *Proceedings of the National Academy of Sciences of the USA* **103**: 1627–1632.

Digiuni S, **Schellmann S**, **Geier F**, ***et al.*** **2008**. A competitive complex formation mechanism underlies trichome patterning in Arabidopsis leaves. *Molecular Systems Biology* **4**: Article 217.

Douady S, **Couder Y. 1996**. Phyllotaxis as a dynamical self organizing process Part III: the simulation of the transient regimes of ontogeny. *Journal of Theoretical Biology* **178**: 295–312.

Draelants D, **Broeckhove J**, **Beemster GTS**, **Vanroose W. 2013**. Numerical bifurcation analysis of the pattern formation in a cell based auxin transport model. *Journal of Mathematical Biology* **67**: 1279–1305.

Dumais J, **Harrison LG. 2000**. Whorl morphogenesis in the dasycladalean algae: the pattern formation viewpoint. *Philosophical Transactions of the Royal Society of London* **B355**: 281–305.

Farcot E, **Yuan Y. 2013**. Homogeneous auxin steady states and spontaneous oscillations in flux-based auxin transport models. *SIAM Journal of Applied Dynamical Systems* **12**: 1330–1353.

Feugier FG, **Mochizuki A**, **Iwasa Y. 2005**. Self-organizing formation of vascular system of plant leaves: co-orientation between auxin flux and pump proteins. *Journal of Theoretical Biology* **236**: 366–375.

Friml J. 2003. Auxin transport–shaping the plant. *Current Opinion in Plant Biology* **6**: 7–12.

Fujita H, **Toyokura K**, **Okada K**, **Kawaguchi M. 2011**. Reaction–diffusion mechanism in shoot apical meristem of plants. *PLoS ONE* **6**: e18243.

Furutani M, **Nakano Y**, **Tasaka M. 2014**. MAB4-induced auxin sink generates local auxin gradients in *Arabidopsis* organ formation. *Proceedings of the National Academy of Sciences of the USA* **111**: 1198–1203.

Gierer A, **Meinhardt H. 1972**. A theory of biological pattern formation. *Kybernetik* **12**: 30–39.

Guenot B, **Bayer E**, **Kierzkowski D**, ***et al.*** **2012**. PIN1-independent leaf initiation in *Arabidopsis*. *Plant Physiology* **159**: 1501–1510.

Hakman I, **Hallberg H**, **Palovaraa J. 2009**. The polar auxin transport inhibitor NPA impairs embryo morphology and increases expression of an auxin efflux facilitator protein PIN during *Picea abies* somatic embryo development. *Tree Physiology* **29**: 483–496.

Harrison LG. 1993. *Kinetic theory of living pattern*. Cambridge: Cambridge University Press.

Harrison LG. 2011. *The shaping of life*. Cambridge: Cambridge University Press.

Harrison LG, **Kolář M. 1988**. Coupling between reaction–diffusion prepattern and expressed morphogenesis, applied to desmids and dasyclads. *Journal of Theoretical Biology* **130**: 493–515.

Harrison LG, **von Aderkas P. 2004**. Spatially quantitative control of the number of cotyledons in a clonal population of somatic embryos of hybrid larch *Larix* × *leptoeuropaea*. *Annals of Botany* **93**: 423–434.

Harrison LG, **Snell J**, **Verdi R**, **Vogt DE**, **Zeiss GD**, **Green BR. 1981**. Hair morphogenesis in *Acetabularia mediterranea*: temperature-dependent spacing and models of morphogen waves. *Protoplasma* **106**: 211–221.

Harrison LG, **Graham KT**, **Lakowski BC. 1988**. Calcium localization during *Acetabularia* whorl formation: evidence supporting a two-stage hierarchical mechanism. *Development* **104**: 255–262.

Harrison LG, **Donaldson G**, **Lau W**, ***et al.*** **1997**. CaEGTA uncompetitively inhibits calcium activation of whorl morphogenesis in *Acetabularia*. *Protoplasma* **196**: 190–196.

Harrison LG, **Wehner S**, **Holloway DM. 2001**. Complex morphogenesis of surfaces: theory and experiment on coupling of reaction-diffusion to growth. *Faraday Discussions* **120**: 277–294.

He F, **Wei C**, **Wu H**, **Cheung D**, **Jiao R**, **Ma J. 2015**. Fundamental origins and limits for scaling a maternal morphogen gradient. *Nature Communications* **6**: 6679.

Herschkowitz-Kaufman M. 1975. Bifurcation analysis of nonlinear reaction-diffusion equations II. Steady-state solutions and comparison with numerical simulations. *Bulletin of Mathematical Biology* **37**: 589–636.

Holloway DM, **Harrison LG. 1995**. Order and localization in reaction–diffusion pattern. *Physica A* **222**: 210–233.

Holloway DM, **Harrison LG. 1999**. Algal morphogenesis: modelling interspecific variation in *Micrasterias* with reaction-diffusion patterned catalysis of cell surface growth. *Philosophical Transactions of the Royal Society of London* **B354**: 417–433.

Holloway DM, **Harrison LG. 2008**. Pattern selection in plants: coupling chemical dynamics to surface growth in three dimensions. *Annals of Botany* **101**: 361–374.

Holloway DM, **Harrison LG**, **Kosman D**, **Vanario-Alonso CE**, **Spirov AV. 2006**. Analysis of pattern precision shows that *Drosophila* segmentation develops substantial independence from gradients of maternal gene products. *Developmental Dynamics* **235**: 2949–2960.

Holloway DM, **Brook B**, **Kang J**, **Wong C**, **Wu M. 2016**. A quantitative study of cotyledon positioning in conifer development. *Botany* **94**: 1063–1074.

Houchmandzadeh B, **Wieschaus E**, **Leibler S. 2002**. Establishment of developmental precision and proportions in the early *Drosophila* embryo. *Nature* **415**: 798–802.

Hunding A. 1987. Bifurcations in Turing systems of the second kind may explain blastula cleavage plane orientation. *Journal of Mathematical Biology* **25**: 109–122.

Jönsson H, **Heisler MG**, **Reddy GV**, ***et al.* 2005**. Modeling the organization of the WUSCHEL expression domain in the shoot apical meristem. *Bioinformatics* **21** (Suppl.): i232–i240.

Jönsson H, **Heisler MG**, **Shapiro BE**, **Mjolsness E**, **Meyerowitz EM. 2006**. An auxin-driven polarized transport model for phyllotaxis. *Proceedings of the National Academy of Sciences of the USA* **103**: 1633–1638.

Kitazawa MS, **Fujimoto K. 2015**. A dynamical phyllotaxis model to determine floral organ number. *PLoS Computational Biology* **11**: e1004145.

Lacalli TC. 1981. Dissipative structures and morphogenetic pattern in unicellular algae. *Philosophical Transactions of the Royal Society of London* **B294**: 547–588.

Larsson E, **Sitbon F**, **Ljung K**, **von Arnold S. 2008**. Inhibited polar auxin transport results in aberrant embryo development in Norway spruce. *New Phytologist* **177**: 356–366.

Larsson E, **Roberts CJ**, **Claes AR**, **Franks RG**, **Sundberg E. 2014**. Polar auxin transport is essential for medial versus lateral tissue specification and vascular-mediated valve outgrowth in *Arabidopsis* gynoecia. *Plant Physiology* **166**: 1998–2012.

Logg A, **Wells GN. 2010**. DOLFIN: automated finite element computing. *ACM Transactions on Mathematical Software* **37**: Article 20.

Logg A, **Wells GN**, **Hake J. 2012**. DOLFIN: a C++/Python finite element library. In Logg A, Mardal K-A, Wells GN, eds. *Automated solution of differential equations by the finite element method*. Springer, Lect. Notes in Comp. Sci. and Eng. **84**, 173–225.

Meinhardt H. 1982. *Models of biological pattern formation*. London: Academic Press.

Mitchison GJ. 1981. The polar transport of auxin and vein patterns in plants. *Philosophical Transactions of the Royal Society of London* **B295**: 461–471.

Nagata W, **Harrison LG**, **Wehner S. 2003**. Reaction–diffusion models of growing plant tips: bifurcations on hemispheres. *Bulletin of Mathematical Biology* **65**: 571–607.

Nagata W, **Zangeneh HRZ**, **Holloway DM. 2013**. Reaction–diffusion patterns in plant tip morphogenesis: bifurcations on spherical caps. *Bulletin of Mathematical Biology* **75**: 2346–2371.

Nicolis G, **Prigogine I. 1977**. *Self-organization in nonequilibrium systems*. New York: Wiley.

Prigogine I, **Lefever R. 1968**. Symmetry-breaking instabilities in dissipative systems. II. *Journal of Chemical Physics* **48**: 1695–1700.

Raspopovic J, **Marcon L**, **Russo L**, **Sharpe J. 2014**. Digit patterning is controlled by a Bmp-Sox9-Wnt Turing network modulated by morphogen gradients. *Science* **345**: 566–570.

Reinhardt D, **Mandel T**, **Kuhlemeier C. 2000**. Auxin regulates the initiation and radial position of plant lateral organs. *Plant Cell* **12**: 507–518.

Rolland-Lagan A-G, **Prusinkiewicz P. 2005**. Reviewing models of auxin canalization in the context of leaf vein pattern formation in *Arabidopsis. Plant Journal* **44**: 854–865.

Rozada I, **Ruuth S**, **Ward MJ. 2013**. The stability of localized spot patterns for the Brusselator on the sphere. *SIAM Journal of Applied Dynamical Systems* **13**: 564–627.

Salazar-Ciudad I, **Jernvall J**, **Newman SA. 2003**. Mechanisms of pattern formation in development and evolution. *Development* **130**: 2027–2037.

Sheth R, **Marcon L**, **Bastida MF**, ***et al.* 2012**. Hox genes regulate digit patterning by controlling the wavelength of a Turing-type mechanism. *Science* **338**: 1476–1480.

Sick S, **Rinker S**, **Timmer J**, **Schlake T. 2006**. WNT and DKK determine hair follicle spacing through a reaction-diffusion mechanism. *Science* **314**: 1447–1450.

Smith RS, **Guyomarc'h S**, **Mandel T**, **Reinhardt D**, **Kuhlemeier C**, **Prusinkiewicz P. 2006**. A plausible model of phyllotaxis. *Proceedings of the National Academy of Sciences of the USA* **103**: 1301–1306.

Turing AM. 1952. The chemical basis of morphogenesis. *Philosophical Transactions of the Royal Society of London* **B237**: 37–72.

van Mourik S, **Kaufmann K**, **van Dijk ADJ**, **Angenent GC**, **Merks RMH**, **Molenaar J. 2012**. Simulation of organ patterning on the floral meristem using a polar auxin transport model. *PLoS ONE* **7**: e28762.

von Aderkas P. 2002. *In vitro* phenotypic variation in larch cotyledon number. *International Journal of Plant Sciences* **163**: 301–307.